SCIENCE CHINA
Physics, Mechanics & Astronomy

•Article•

December 2020 Vol. 63 No. 12: 124611
https://doi.org/10.1007/s11433-020-1610-8

The intrinsic nature of materials failure and the global non-equilibrium energy criterion

Biao Wang*

School of Physics and Sino-French Institute of Nuclear Engineering and Technology, Sun Yat-sen University, Guangzhou 510275, China

Received July 28, 2020; accepted August 10, 2020; published online October 23, 2020

Materials failure under some sort of loading is a well-known natural phenomenon, and the reliable prediction of materials failure is the most important key issue for many different kinds of engineering structures based on their safety considerations. In this research, instead of establishing empirical models, the material failure process was modeled as a nonequilibrium process based on the microstructural mechanism. Then, the evolution equations were established and the stability analysis was carried out to obtain the critical conditions for the materials failure. It was found that the material strength was a global property in nature, and the commonly used local criteria based on the most dangerous point failure were not the rational assumption. Based on the idea, some examples were considered, such as the size effect of the material strength, the strength of the polycrystalline metals, the stress-strain relationship of the ultrafine crystalline metal with nanoscale growth twins, the strength of lithium niobite crystal specimens with notches. All of the theoretical predictions gave reasonable results compared with the experimental data.

strength theory, nonequilibrium thermodynamics, stability analysis, size effect, nanomaterials

PACS number(s): 46.05.+b, 62.20.Mk, 62.20.Fe, 05.70.Ln

Citation: B. Wang, The intrinsic nature of materials failure and the global non-equilibrium energy criterion, Sci. China-Phys. Mech. Astron. **63**, 124611 (2020), https://doi.org/10.1007/s11433-020-1610-8

1 Introduction

Material breakages or failures under loading are very common natural phenomena, and how to establish the criterion of material breakdown has attracted much attention from physicists, material scientists, earth scientists, and mechanical and civil engineers in particular, for a very long time. In essence, the strength theory of materials is the failure criterion of a material. da Vinci (1452-1519) and Galilei (1562-1642) may be the earliest researchers of the problem. They performed tensile and bending tests of wires and stones to determine their strength. da Vinci believed that the strength of an iron wire depended significantly on its length, while Galilei believed that fracturing occurred when a critical stress was reached. To satisfy widespread engineering needs, various strength theories have been established for different materials. A general common characteristic of all the strength theories is that when some stresses or stress combinations at some point in a material specimen reach a critical value, the material sample will break. The critical values for different materials have been measured using some standard small samples, and these values have been tabulated in technical handbooks. A specific characteristic for the classical strength theory is based on the essential belief that material failure behavior is a local phenomenon; i.e., the most dangerous point will fail independently when a local strength criterion is satisfied. The neighboring points only affect the stress distributions in the specimen.

These classical strength criteria can generally be treated as empirical criteria based on the experience and the vast ex-

*Corresponding author (email: wangbiao@mail.sysu.edu.cn)

perimental data. It is a well-known fact that in some cases, the predictions by these classical strength theories face significant discrepancies with the experimental results for different kinds of materials. Engineers have to use some significantly large safety factors to consider uncertainty when they carry out the design of some structures. Generally speaking, since the ultimate strength of metals changes inversely with the fracture toughness for many kinds of materials, the higher the strength of the material is, the lower the fracture toughness is. Therefore, in the 1940s, catastrophic failures happened in many ships, bridges, and the other constructions based on the ultimate strength design due to the lower fracture toughness of the materials used to build these structures. To solve the strength problem for the materials and structures with some sort of existing cracks, fracture mechanics was established. Fracture mechanics plays an extremely important role and is well accepted in both academic society and engineering society. In fact, fracture mechanics was initiated by Griffith [1] in 1921. Griffith considered the phenomena of rupture and flow in solids using a flat glass plate as an example. If a crack exists in a continuum body, the maximum stress at the crack tip exhibits some singularity and approaches infinity for any non-zero applied loading. Of course, if the applied loading is very small and the crack length is very tiny, the specimen will not break. To solve such a contradiction, the energy release rate and some related energy criteria were established that provided very reliable tools for engineers to evaluate the strength of materials with cracks. Recently, many nanomaterials have been successfully fabricated and the size effect of material strength has become more enhanced. For example, if the grain size of nano-grained Cu decreases below 100 nm, the tensile yielding strength may become ten times larger than that of coarse-grained copper [2]. Recently, it has become possible to obtain flawless or near-flawless material. The theoretical prediction of ideal material strength based on chemical bonds also faces many challenges. For example, the ideal strength of carbon fiber was predicted to be about 180 GPa, but the experimental measurements for carbon whiskers or the fibers ranged from about 2% to about 10% of the ideal strength. Although most scholars believed that the departure was attributed to the existing defects in the fibers, many uncertainties in the theoretical prediction for the ideal strength were also very obvious. Many researchers used the first-principle calculation to obtain the theoretical strength values for some ideal materials. The basic criterion mainly depended on the total energy release of the chemical bonds breaking [3].

In the present work, based on the failure mechanism, the failure process was modeled as a nonequilibrium process [4], the changing rates of some microstructural parameters played the role of the "flows" of the failure process, and their conjugate forces served as the driving forces to induce the failure. Thus, the thermodynamic evolution equations of the failure process were established. With a stability analysis, one could establish the condition for the loss of the stability of the failure process, which was equivalent to the failure criterion of the material. It was found that for the material with an existing crack, the criterion gave the same result as the energy release rate criterion. Based on the established energy criterion and dimensional analysis, a general size effect of the strength was also derived and compared with the extensive experimental data. As another example, the stress-strain relationship, the strength of the polycrystalline metals, and the ultrafine crystalline metal with nanoscale growth twins were used. It was found that the strength property was indeed a global behavior of the specimen; i.e., when the external loading reached its critical value, all of the points in the specimen were correlated with each other.

This methodology for evaluating the material strength or the failure property could also be defined as the virtual process energy criterion (VPEC). First of all, one needed to identify or assume the failure process, then choose some microstructural parameters to describe the process, and then derive the free energy change and establish the non-equilibrium evolution equations. The failure properties such as the strength of the materials could be determined from these equations.

To explain the difference between the local and global strength theory, the recent experimental results on the strength of lithium niobite crystal specimens with different sizes of notches obtained by our group were used.

2 Global non-equilibrium energy criterion

When considering a material specimen under some sort of external loading, when the load is small, the specimen will deform elastically without any energy dissipation, or the entropy production. By increasing the external load, some sort of defects will be created or activated in the specimen, thus inducing entropy production. Based on the non-equilibrium thermodynamics [4], it is known that the changing rate of the microstructural defect parameters can be defined as the "flow" of the process, and the conjugate driving force is the derivative of the entropy production with respect to the corresponding defect parameter. In other words, if the defect parameters can be denoted as a_i, the conjugate driving force can be denoted as F_i. The first law of thermodynamics can be expressed as:

$$\delta Q = \mathrm{d}U - \delta W, \quad \delta W = \iint_{\Gamma} \Pi_i \delta u_i \mathrm{d}s, \tag{1}$$

where $\mathrm{d}U$ is the internal energy increment. For our static problems, $\mathrm{d}U$ might refer to the elastic strain energy, δW is the environment work on the system, Π_i, u_i, Γ refer the force

and displacements components along the boundary Γ, and δQ is the heat supplied to the system.

For a non-equilibrium process, the state function, entropy S, is introduced, and it can be divided into the exchange entropy due to the exchange with the environment and irreversible entropy production, as shown below:

$$\mathrm{d}S = \mathrm{d}S_r + \mathrm{d}S_i, \quad \mathrm{d}S_r = \frac{\delta Q}{T}, \quad \mathrm{d}S_i \geq 0, \tag{2}$$

which is also a state of the second law of thermodynamics. By combining eqs. (1) and (2), one can derive

$$\begin{aligned}\mathrm{d}S_i &= \mathrm{d}S - \mathrm{d}S_r = \mathrm{d}S - \frac{\delta Q}{T} = \mathrm{d}S - \frac{1}{T}(\mathrm{d}U - \delta W) \\ &= -\frac{1}{T}(\mathrm{d}U - \delta W - T\mathrm{d}S).\end{aligned} \tag{3}$$

By introducing the definition of the Gibbs free energy, one can write

$$G = U - W - ST. \tag{4}$$

Its variation can be written in the form shown below:

$$\begin{aligned}\mathrm{d}G &= \mathrm{d}U - \iint_{\Gamma} \delta(\Pi_k u_k)\mathrm{d}A - \mathrm{d}(ST) \\ &= \mathrm{d}U - \iint_{\Gamma} \Pi_k \delta u_k \mathrm{d}A - \iint_{\Gamma} u_k \delta \Pi_k \mathrm{d}A - T\mathrm{d}S - S\mathrm{d}T.\end{aligned} \tag{5}$$

By combining the above equation with eq. (3), one can establish

$$\begin{aligned}&\mathrm{d}S_i = -\frac{1}{T}\left(\mathrm{d}G + \iint_{\Gamma} u_k \delta \Pi_k \mathrm{d}s + S\mathrm{d}T\right) = -\frac{1}{T}\mathrm{d}G; \\ &\delta \Pi_k = 0, \ \mathrm{d}T = 0.\end{aligned} \tag{6}$$

It is very clear that in deriving eq. (6), it is assumed that under the condition of keeping the external loading and temperature constant, the entropy production can be expressed as the decrease of the Gibbs free energy.

According to the non-equilibrium thermodynamics, if the entropy production is due to the defect creation and evolution, the thermodynamic driving force can be expressed in the following form:

$$F_k = \frac{\partial S_i}{\partial a_k} = -\frac{1}{T}\frac{\partial G}{\partial a_k}. \tag{7}$$

Its conjugate "flow" can be expressed as:

$$\frac{\mathrm{d}a_k}{\mathrm{d}t} = \lambda_k F_k = -\frac{\lambda_k}{T}\frac{\partial G}{\partial a_k}. \tag{8}$$

In fact, for a general non-equilibrium process not very far from equilibrium state, it is a well-known fact that the "flow" is linearly related to its energy driving force [4]. At the least, it is a well-known assumption. Thus, we could establish the evolution equation of the damaged microstructures of the material under the external loading. To determine the strength of the material specimen, generally speaking, it is not necessary to derive the solution of the evolution equation. If one can establish the stability condition of the evolution equation, the critical condition gives the strength of the material specimen. This was our basic idea of how to evaluate the material strength. In other words, based on the failure mechanism, by choosing a proper parameter to represent the "flow" of the system, one can establish the non-equilibrium energy evolution equation, from which one can obtain the critical failure conditions of the materials. Compared with the classical strength theory, the energy criterion is a global, rational criterion. In fact, for most cases, one can decide if an equilibrium state is stable or not by using the second-order variation of the Gibbs free energy. If it is larger than zero, that means any perturbation will increase the free energy, the state is stable, whereas, if it is smaller than zero, any perturbation will make the free energy decrease, this process will continue spontaneously, and such a state is unstable. Therefore, one can establish the strength criterion by setting the second-order variation of the Gibbs free energy equal to zero without need to consider the evolution equations with time. In the following sections, we use some examples to show how to use the formalism for material failure problems.

3 Some examples

3.1 A crack in an infinite body

In such a case, the crack length can be treated as the microstructural parameter. Its rate can be treated as the "flow":

$$\frac{\mathrm{d}a}{\mathrm{d}t} = -\frac{\lambda}{T}\frac{\delta G}{\delta a} = -\frac{\lambda}{T}\frac{\delta(E+\Lambda)}{\delta a} = 0, \tag{9}$$

where E refers to the elastic Gibbs free energy and Λ refers to the resistant part of the free energy, such as the surface energy, and plastic dissipation energy. For the steady state, eq. (9) gives the same result as the energy release rate criterion given by Griffith. It is a well-known fact that the energy release rate criterion is a global criterion. It depends on the total released energy of a whole specimen. If one assumes that the resistant part of the free energy Λ also depends on the crack length, one needs to evaluate the second-order derivative to judge when the crack propagation will lose its stability.

3.2 Size effect of strength using the dimensional analysis

The strength of materials, especially brittle materials, depends on their size. Generally speaking, the larger a specimen is, the smaller its strength is. Usually, it is assumed that random defects exist in a specimen, and extreme statistics are used to obtain the size effect of the strength. Additionally, the Weibull distribution of the strength can be derived for brittle materials. Extensive investigations have been carried out on the size effects for different materials [5,6]. Based on the energy criterion, and using the dimensional analysis [7], the

author derived the size effect of the strength for general materials.

3.2.1 The size effect of the strength of an infinite body with a finite crack size

For a crack with the area S in an infinite body, the dimensions of the length, mass, and time are set as L, M, and t, respectively. The dimension of stress σ can be derived as $ML^{-1}t^{-2}$, the strain ε is dimensionless, and the dimension of the resistant energy R per unit area is Mt^{-2}. We assumed that the released energy per unit propagation area of the crack could be expressed in the form shown below:

$$G = f(\varepsilon)\sigma^{\alpha}S^{\beta}. \tag{10}$$

Based on the energy criterion, the substitution of the dimensions of all the variables yielded,

$$G = R \Rightarrow f(\varepsilon)(ML^{-1}t^{-2})^{\alpha}L^{2\beta} = Mt^{-2}. \tag{11}$$

From eq. (11), one could derive,

$$\alpha = 1, \beta = \frac{1}{2}. \tag{12}$$

Thus, one could establish the relationship of the strength with the crack area, as follows:

$$\sigma \propto S^{-1/2}, \tag{13}$$

which was the same as the result of the fracture mechanics, and irrelevant to the material properties.

3.2.2 The size effect of the strength of a finite body

It is assumed that the free energy drop accompanies some defect creation or propagation in the material can be expressed as follows:

$$G = f(\varepsilon)\sigma^{\alpha}V^{\beta}, \tag{14}$$

where V is the volume of a specimen.

For different failure mechanisms, the dimension of the resistant energy may be different, which can be discussed as follows.

(1) For a ductile material, the failure process is usually due to the growth of voids. Thus, the dimension of the resistant energy per unit volume is $R=ML^{-1}t^{-2}$. According to the energy criterion, one can establish

$$G = R \Rightarrow f(\varepsilon)(ML^{-1}t^{-2})^{\alpha}L^{3\beta} = ML^{-1}t^{-2}. \tag{15}$$

One can find α=1, β=0. This means that for such a failure mechanism of the ductile material, no obvious size effect can be found, which has also been proven with extensive experimental data.

(2) If the material fails due to some sort of area-defect, such as a crack, the dimension of the resistant energy per unit area is $R=Mt^{-2}$. One can find

$$f(\varepsilon)(ML^{-1}t^{-2})^{\alpha}L^{3\beta} = Mt^{-2}. \tag{16}$$

One can derive

$$\alpha = 1, \ \beta=1/3. \tag{17}$$

Then

$$\sigma \propto V^{-1/3}. \tag{18}$$

(3) If the material fails due to the propagation of a line or point defect, the dimension of the resistant energy per unit length is $R=MLt^{-2}$, and one can establish

$$f(\varepsilon)(ML^{-1}t^{-2})^{\alpha}L^{3\beta} = MLt^{-2}. \tag{19}$$

One can obtain

$$\alpha = 1, \quad \beta=2/3, \tag{20}$$

$$\sigma \propto V^{-2/3}. \tag{21}$$

In summary, if the power law of the size effect of the strength is valid, based on the energy criterion, the general power exponents are found by dimensional analysis. Based on the published experimental data [8-11] for different materials, the power law of the size effect of the strength seems well established, whereas the exponents can vary to a large extent, as shown below.

(i) The size effect of the nominal strength of notched specimens of graphite/epoxy fiber composite laminate

Bažant et al. [8] carried out the measurement of the size effect of the nominal strength of notched specimens of graphite/epoxy crossly and quasi-isotropic fiber composite laminates. Their results are shown in Figure 1 along with the power-law fitting curve.

(ii) The size effect on the compressive failure of concrete

Vu et al. [9] investigated the size effect on the compressive failure of heterogeneous materials. The materials were mainly concrete materials. Their experimental results are shown in Figure 2, along with the power-law fitting curve.

(iii) The size effect in ceramic fractures with different toughening effects

For ceramics and ceramic composites with different toughening mechanisms, such as crack deflection, Zdeněk and Kazemi [10] carried out an investigation on the size effect in a fracture. Their results are shown in Figure 3.

(iv) The size effect on the shear behavior of the rock joints

Bandis et al. [11] carried out experimental studies of the size effect on the shear strength of rock joints. Their results are shown as in Figure 4.

3.3 Some general characteristics of the plastic and failure behaviors of polycrystalline metals

Plastic deformation and high ductility are the main characteristics of polycrystalline metals. To satisfy both academic and engineering demands, extensive investigations have been carried out from various aspects of view, such as in the previous study conducted by Wang and Boehler [12]. Based on the methodology developed above, the author established a quantitative plastic evolution model, from which

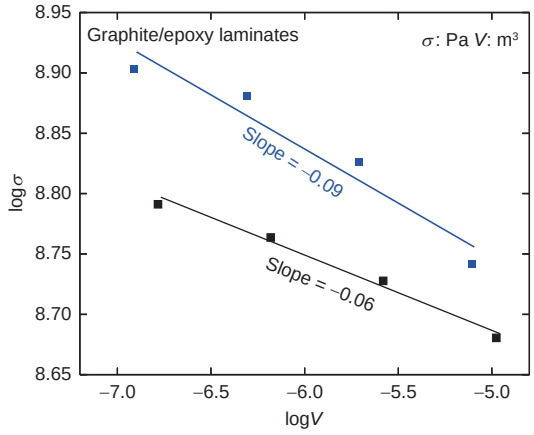

Figure 1 (Color online) The graphite/epoxy laminates with different sizes were stretched at room temperature, and the relationships between the strength and volume were fitted to a logarithmic scale. The black dots represent the double-edge notched crossply specimens, and the blue dots represent the single-edge notched quasi-isotropic specimens.

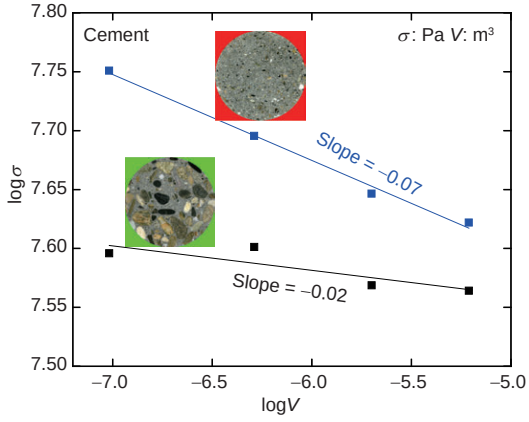

Figure 2 (Color online) Two formulations of cement were sintered into cylinders with different volumes and compressed at room temperature.

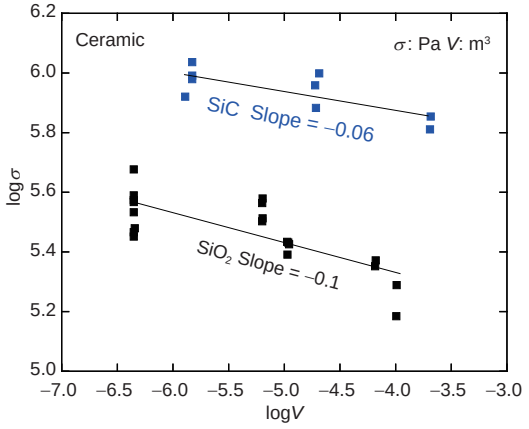

Figure 3 (Color online) The logarithmic relationship between the strength and volume of ceramic under Mode I fracture loading.

one can derive some general characteristics for the plastic and failure behaviors. Then focusing on the stress-strain relationship and the strength of an ultrafine crystalline metal with nanoscale growth twins, and the predicted results were compared with the available experimental data.

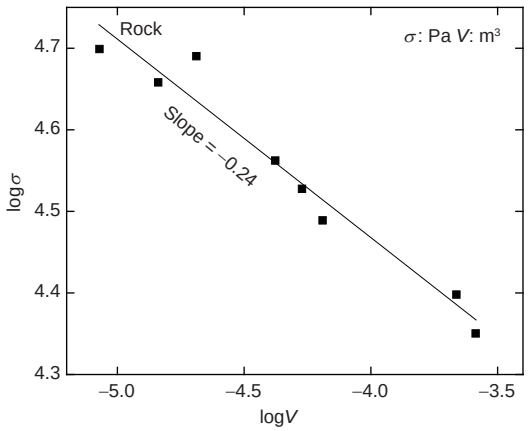

Figure 4 The logarithmic relationship between the shear strength and the volume of a specimen.

It is well known that when a polycrystalline metal specimen is subjected to some sort of external loading, it will deform elastically, and when the load reaches some critical value, some favorable slip systems will become active and induce plastic deformation. With the occurrence of the plastic deformation, the elastic Gibbs free energy will change, and energy dissipation related to the slip resistance can be created. I derived the total free energy change using eigenstrain methodology [13], as follows.

Considering a polycrystalline metal specimen under external loading σ_{ij}^0, the elastic Gibbs free energy can be written in the form shown below:

$$W_0 = \frac{1}{2}\iiint_D \sigma_{ij}^0 \varepsilon_{ij}^0 \mathrm{d}v - \iint_\Gamma F_i^0 u_i^0 \mathrm{d}s. \tag{22}$$

When the load reaches a critical value, the irreversible slips induce plastic deformation $\varepsilon_{ij}^p(\mathbf{x})$, and the elastic Gibbs free energy can be written in the form shown below:

$$\begin{aligned} W &= \frac{1}{2}\iiint_D (\sigma_{ij}^0 + \sigma_{ij})(\varepsilon_{ij}^0 + \varepsilon_{ij} - \varepsilon_{ij}^p)\mathrm{d}v \\ &\quad - \iint_\Gamma F_i^0 (u_i^0 + u_i)\mathrm{d}s \\ &= \frac{1}{2}\iiint_D (\sigma_{ij}^0 + \sigma_{ij})(\varepsilon_{ij}^0 + \varepsilon_{ij} - \varepsilon_{ij}^p)\mathrm{d}v \\ &\quad - \iint_\Gamma \sigma_{ij}^0 n_j (u_i^0 + u_i)\mathrm{d}s, \end{aligned} \tag{23}$$

where $\sigma_{ij}, \varepsilon_{ij}, u_i$ are the perturbations of the stress, strain, and displacement due to the plastic strain. Using Green's function, one can obtain [13]

$$\begin{aligned} &\sigma_{ij}(\mathbf{x}) = C_{ijkl}\iiint_D e_{sth} e_{lnh} C_{pqmn} T_{kp,qt}(\mathbf{x}-\mathbf{x}')\varepsilon_{sm}^p \mathrm{d}v', \\ &e_{sth} e_{lnh} = \delta_{sl}\delta_{tn} - \delta_{sn}\delta_{tl}, \end{aligned} \tag{24}$$

where $T_{kp,qt}(\mathbf{x}-\mathbf{x}')$ is the second-order derivative of Green's function, C_{ijkl} is the elastic moduli tensor, and δ_{sl} is the

Kronecker delta. The elastic Gibbs free energy change due to the occurrence of the plastic deformation can be derived as follows:

$$\Delta W = W - W_0 = -\frac{1}{2}\iiint_D (2\sigma_{ij}^0 + \sigma_{ij})\varepsilon_{ij}^p \mathrm{d}v. \tag{25}$$

In deriving eq. (25), we used the following conditions:

$$\iiint_D \sigma_{ij}^0(\varepsilon_{ij} - \varepsilon_{ij}^p)\mathrm{d}v = \iiint_D \sigma_{ij}(\varepsilon_{ij}^0 + \varepsilon_{ij})\mathrm{d}v = 0. \tag{26}$$

Accompanying the plastic deformation, the slip resistant force will do the work and increase the free energy of the system. Since we only needed to consider some general characteristics of the plastic deformation, we adapted a general form for the resistant free energy in unit volume $\Delta[\varepsilon_{kl}^p(\mathbf{x})]$, which is a function of the plastic strains. The total resistant free energy is

$$\Lambda = \iiint_D \Delta[\varepsilon_{kl}^p(\mathbf{x})]\mathrm{d}v. \tag{27}$$

The substitution of eqs. (25) and (27) into eq. (8) gives the evolution equation of the plastic deformation

$$\frac{\mathrm{d}\varepsilon_{ij}^p}{\mathrm{d}t} = -\lambda\frac{\delta(\Delta W + \Lambda)}{\delta\varepsilon_{ij}^p} = \lambda\left(\sigma_{ij}^0 + \sigma_{ij} - \frac{\mathrm{d}\Delta}{\mathrm{d}\varepsilon_{ij}^p}\right). \tag{28}$$

For the equilibrium state, the evolution velocity is zero, and one obtains

$$\begin{aligned}&\sigma_{ij}^0 + \sigma_{ij} - \frac{\mathrm{d}\Delta}{\mathrm{d}\varepsilon_{ij}^p}\\ &= \sigma_{ij}^0 - \frac{\mathrm{d}\Delta}{\mathrm{d}\varepsilon_{ij}^p} + C_{ijkl}\,e_{sth}\,e_{lnh}C_{pqmn}\iiint_D T_{kp,qt}(\mathbf{x}-\mathbf{x}')\varepsilon_{sm}^p \mathrm{d}v'\\ &= 0.\end{aligned} \tag{29}$$

Eq. (29) is the same as the equilibrium stress condition, from which one can determine the steady plastic deformation. It was not our intention to solve the equation for some specific materials, but some special characteristics predicted by eq. (29) were pursued.

First of all, if the uniform solution of the plastic deformation is assumed, the solution depends on the applied loading and the slip resistant load. To determine the critical load for the specimen failure, one can set the second-order derivative of the total free energy to be equal to zero to obtain the critical value of the plastic strain firstly, as follows:

$$C_{ijkl}\,e_{sth}e_{lnh}C_{pqmn}\iiint_D T_{kp,qt}(\mathbf{x}-\mathbf{x}')\mathrm{d}v' - \frac{\mathrm{d}^2\Delta}{\mathrm{d}\left(\varepsilon_{ij}^p\right)^2} = 0. \tag{30}$$

Then, by substituting into eq. (29), one can obtain the critical load. This is a similar approach to the spinodal analysis for many critical phenomena, such as nucleation and crystallization problems [14]. To investigate the material specific characteristics when the load approaches its critical value σ_{ij}^c, by writing $\Delta\sigma_{ij} = \sigma_{ij}^c - \sigma_{ij}^0$; $\varepsilon_{ij}^p = \varepsilon_{ij}^c + \Delta\varepsilon_{ij}^p$, which indicates a fluctuation from the average value, one needs only to consider the behavior of the fluctuation field. The author did not try to derive the detailed solutions, here the main concern was determining how the plastic zone would develop when the load approached its critical value.

The fluctuation $\Delta\varepsilon_{ij}^p$ is considered a small quantity and $\Delta[\varepsilon_{kl}^p(\mathbf{x})]$ is expanded up to the second-order terms in power of $\Delta\varepsilon_{ij}^p$. By taking the Fourier transform of the last term in eq. (29), and expanding the Fourier transformed $\hat{\mathbf{T}}(\mathbf{k})$ in powers of $|\mathbf{k}|$ and keeping the terms to the second order, since it is not interesting to consider the change of fluctuation distribution shape profile, substitution of all the expressions into eq. (29) yields

$$R^2\nabla^2(\Delta\varepsilon^p) - C(\Delta\varepsilon^p)^2 + \Delta\sigma = 0, \tag{31}$$

where

$$\begin{aligned}R &= M\int_{-\infty}^{\infty}\int_{-\infty}^{\infty}\int_{-\infty}^{\infty}\mathbf{T}(\mathbf{x})[\mathbf{e}(\mathbf{k})\cdot\mathbf{x}]^2\mathrm{d}^3x,\\ C &= \frac{1}{2}\frac{\mathrm{d}^3\Delta}{\mathrm{d}(\varepsilon_{ij}^p)^3}\Big|_{\varepsilon_{ij}^p=\varepsilon_{ij}^c}.\end{aligned} \tag{32}$$

In deriving eq. (31), in order to estimate the special properties predicted by the model, it was assumed that only one component of plastic strain was not zero, and the following equations were also used:

$$\begin{aligned}&\hat{T}_{kp,qt}(\mathbf{k}) = \int_{-\infty}^{\infty}\int_{-\infty}^{\infty}\int_{-\infty}^{\infty}T_{kp,qt}(\mathbf{x})\mathrm{e}^{-\mathrm{i}\mathbf{k}\cdot\mathbf{x}}\mathrm{d}^3x\\ &= \hat{T}_{kp,qt}(|\mathbf{k}|=0) + \frac{\partial\hat{T}_{kp,qt}(\mathbf{k})}{\partial|\mathbf{k}|}\Big|_{|\mathbf{k}|=0}|\mathbf{k}| + \frac{\partial^2\hat{T}_{kp,qt}(\mathbf{k})}{\partial|\mathbf{k}|^2}\Big|_{|\mathbf{k}|=0}|\mathbf{k}|^2 + \cdots\\ &= \int_{-\infty}^{\infty}\int_{-\infty}^{\infty}\int_{-\infty}^{\infty}T_{kp,qt}(\mathbf{x})\mathrm{d}^3x + \mathrm{i}|\mathbf{k}|\int_{-\infty}^{\infty}\int_{-\infty}^{\infty}\int_{-\infty}^{\infty}T_{kp,qt}(\mathbf{x})\mathbf{e}(\mathbf{k})\cdot\mathbf{x}\mathrm{d}^3x\\ &\quad -|\mathbf{k}|^2\int_{-\infty}^{\infty}\int_{-\infty}^{\infty}\int_{-\infty}^{\infty}T_{kp,qt}(\mathbf{x})[\mathbf{e}(\mathbf{k})\cdot\mathbf{x}]^2\mathrm{d}^3x + \cdots\\ &= \int_{-\infty}^{\infty}\int_{-\infty}^{\infty}\int_{-\infty}^{\infty}T_{kp,qt}(\mathbf{x})\mathrm{d}^3x - |\mathbf{k}|^2\int_{-\infty}^{\infty}\int_{-\infty}^{\infty}\int_{-\infty}^{\infty}T_{kp,qt}(\mathbf{x})[\mathbf{e}(\mathbf{k})\cdot\mathbf{x}]^2\mathrm{d}^3x + \cdots,\\ &\mathbf{T}(\mathbf{x}-\mathbf{x}') = \mathbf{T}(\mathbf{x}'-\mathbf{x}),\\ &\sigma_{ij}^c - \frac{\mathrm{d}\Delta}{\mathrm{d}\varepsilon_{ij}^p}\Big|_{\varepsilon_{ij}^p=\varepsilon_{ij}^c} + C_{ijkl}\,e_{sth}e_{lnh}C_{pqmn}\varepsilon_{sm}^c\iiint_D T_{kp,qt}(\mathbf{x}-\mathbf{x}')\mathrm{d}v' = 0,\\ &C_{ijkl}\,e_{sth}e_{lnh}C_{pqmn}\iiint_D T_{kp,qt}(\mathbf{x}-\mathbf{x}')\mathrm{d}v' - \frac{\mathrm{d}^2\Delta}{\mathrm{d}(\varepsilon_{ij}^p)^2}\Big|_{\varepsilon_{ij}^p=\varepsilon_{ij}^c} = 0,\\ &\frac{\mathrm{d}\Delta}{\mathrm{d}\varepsilon_{ij}^p} = \frac{\mathrm{d}\Delta}{\mathrm{d}\varepsilon_{ij}^p}\Big|_{\varepsilon_{ij}^p=\varepsilon_{ij}^c} + \Delta\varepsilon_{ij}^p\frac{\mathrm{d}^2\Delta}{\mathrm{d}(\varepsilon_{ij}^p)^2}\Big|_{\varepsilon_{ij}^p=\varepsilon_{ij}^c}\\ &\qquad + \frac{1}{2}\left(\Delta\varepsilon_{ij}^p\right)^2\frac{\mathrm{d}^3\Delta}{\mathrm{d}(\varepsilon_{ij}^p)^3}\Big|_{\varepsilon_{ij}^p=\varepsilon_{ij}^c} + \cdots.\end{aligned} \tag{33}$$

Following the methodology of refs. [14,15], if one only considers the general profile of the plastic zone, the detailed variations along the angles can be neglected, and eq. (31) becomes

$$R^2\frac{\mathrm{d}^2(\Delta\varepsilon^p)}{\mathrm{d}r^2} - C(\Delta\varepsilon^p)^2 + \Delta\sigma = 0, \tag{34}$$

where the first-order derivative term is neglected, which will only change the shape of the profile. Eq. (34) can be solved analytically, and its solution can be written in the form shown below:

$$\Delta\varepsilon^{p} \sim (\Delta\sigma)^{1/2}\psi(r/\zeta),\ \zeta \sim (\Delta\sigma)^{-1/4}, \tag{35}$$

which means that plastic zone is divergent from the correlation length when the load reaches its critical value. This is also a proof that the failure behavior is a global property, which means that all of the points are closely related to each other at the critical point.

3.4 The stress-strain relationship and the strength of the ultrafine crystalline metal with nanoscale growth twins

For metal materials, generally speaking, the strength of a metal material changes inversely with its ductility; i.e., for those materials with high yielding or ultimate strength, their ductility is generally low. Therefore, finding and fabricating a metal material with both high strength and good ductility is a long-held desire for material scientists. Recently, significant progress has been made in this area. One methodology involves fabricating ultrafine grain metal with nanoscale growth twins inside the grains [16]. The effect can be even more enhanced by creating a gradient nano-twinned structure [17]. A clear understanding based on the large-scale molecular dynamics simulation has been given in ref. [18]. According to the Hall-Petch relation, if the grain size of crystalline metal is reduced, its yielding strength will increase according to the power law with the exponent $-1/2$. For metal with a nanoscale grain size, the dislocation movement may be blocked efficiently by the grain boundaries. Thus, the material may have a much higher strength, but its ductility will become much lower than that of a coarse-grain counterpart. In contrast, for metal materials with comparatively larger grains, by introducing growth twins with tens of nanometer thicknesses inside the grains, the dislocation can move favorably along the twin boundaries because the slip resistance across the boundaries (called the hard slip mode) is three to five times higher than that along the boundaries (called the soft slip mode) [19]. For such a material structure, it was found that high strength and good ductility could be achieved to some extent. Another methodology involving fabricating a high-entropy alloy is not discussed in this manuscript. To simplify the model for the energy dissipation mechanism, it was assumed that in each grain, only one type of nanoscale twin existed, and that the slip displacement under the loading occurred first along the twin boundary direction. Then, with the load increasing and dislocations accumulating, the slip across the twins might occur.

By considering one representative grain in a crystalline metal under an applied loading σ_{ij}^{0} equal to the average stress, if the average plastic strain is denoted as $\bar{\varepsilon}_{kl}^{p}$, the misfit plastic strain inside the grain from its average value can be modeled as the eigenstrain $\varepsilon_{kl}^{*} = \varepsilon_{kl}^{p} - \bar{\varepsilon}_{kl}^{p}$ [13] based on its average value, and one can establish the elastic Gibbs free energy change due to the eigenstrain as follows:

$$W = -\frac{1}{2}\int_{\Omega}[\boldsymbol{\sigma} + 2\boldsymbol{\sigma}^{0}]\boldsymbol{\varepsilon}^{*}\mathrm{d}v = -\frac{1}{2}\int_{\Omega}\left[\sigma_{ij} + 2\sigma_{ij}^{0}\right]\varepsilon_{ij}^{*}\mathrm{d}v, \tag{36}$$

where σ_{ij} represents the stress perturbation inside the grain and is given as follows:

$$\begin{aligned}\sigma_{ij} &= C_{ijkl}(S_{klmn} - I_{klmn})\varepsilon_{mn}^{*} \\ &= C_{ijkl}(S_{klmn} - I_{klmn})(\varepsilon_{mn}^{p} - \bar{\varepsilon}_{mn}^{p}),\end{aligned} \tag{37}$$

for which the author followed the self-consistent approach in order to consider the interaction among different grains. S_{klmn}, I_{klmn} are Eshelby's tensor for a spherical grain and the Identity tensor, respectively, which are shown in Appendix.

For the grain metal with one type of nanoscale twins, since the slip resistance along the twin boundary is far less than the slip resistances across the twin boundary, the slip systems will become active in order. Thus, the plastic strain inside the grain can be expressed in the form shown below:

$$\varepsilon_{kl}^{p} = \sum_{\beta=1}^{3}\gamma^{\beta}\alpha_{kl}^{\beta} + \sum_{\beta=4}^{12}\gamma^{\beta}\alpha_{kl}^{\beta},\ \ \alpha_{kl}^{\beta} = \frac{1}{2}\left(m_{k}^{\beta}n_{l}^{\beta} + m_{l}^{\beta}n_{k}^{\beta}\right), \tag{38}$$

where $m_{k}^{\beta}, n_{l}^{\beta}$ represent a unit vector normal to either the slip plane or the twin boundary plane, and the slip direction. During the slip process, the cohesive energy will create the resistant force to block the slip, thus increasing the Gibbs energy $\Lambda(\boldsymbol{\varepsilon}^{p})$.

The total Gibbs free energy is the sum shown below:

$$G = W + \Lambda, \tag{39}$$

which is a function of the plastic strain and the external field. By keeping the external field and the temperature unchanged, the non-equilibrium evolution equation can be established as follows:

$$\begin{aligned}\frac{\mathrm{d}\gamma^{\beta}}{\mathrm{d}t} &= -\lambda_{1}\frac{\delta G}{\delta\gamma^{\beta}} = -\lambda_{1}\left(\frac{\delta W}{\delta\gamma^{\beta}} + \frac{\delta\Lambda}{\delta\gamma^{\beta}}\right) \\ &= \lambda_{1}\left[\left(\sigma_{ij}^{0} + \sigma_{ij}\right)\alpha_{ij}^{\beta} - \tau_{1}^{p}\right],\ \ 1 \le \beta \le 3, \\ \frac{\mathrm{d}\gamma^{\beta}}{\mathrm{d}t} &= -\lambda_{2}\frac{\delta G}{\delta\gamma^{\beta}} = -\lambda_{2}\left(\frac{\delta W}{\delta\gamma^{\beta}} + \frac{\delta\Lambda}{\delta\gamma^{\beta}}\right) \\ &= \lambda_{2}\left[\left(\sigma_{ij}^{0} + \sigma_{ij}\right)\alpha_{ij}^{\beta} - \tau_{2}^{p}\right],\ \ 4 \le \beta \le 12,\end{aligned} \tag{40}$$

where λ_{1}, λ_{2} are the material constants, or mobility, and

$$\begin{aligned}\tau_{1}^{p} &= \frac{\delta\Lambda}{\delta\gamma^{\beta}},\quad 1 \le \beta \le 3, \\ \tau_{2}^{p} &= \frac{\delta\Lambda}{\delta\gamma^{\beta}},\quad 4 \le \beta \le 12.\end{aligned} \tag{41}$$

Eq. (40) then becomes

$$\frac{\mathrm{d}\gamma^{\beta}}{\mathrm{d}t}=\lambda_1\left[\left(\sigma_{ij}^{0}+\sigma_{ij}\right)\alpha_{ij}^{\beta}-\tau_1^{p}\right]=\lambda_1\left\{\alpha_{ij}^{\beta}\left[\sigma_{ij}^{0}+C_{ijkl}(S_{klmn}-I_{klmn})\left(\sum_{\beta=1}^{3}\gamma^{\beta}\alpha_{mn}^{\beta}+\sum_{\beta=4}^{12}\gamma^{\beta}\alpha_{mn}^{\beta}-\bar{\varepsilon}_{mn}^{p}\right)\right]-\tau_1^{p}\right\},\ 1\le\beta\le 3,$$
$$\frac{\mathrm{d}\gamma^{\beta}}{\mathrm{d}t}=\lambda_2\left[\left(\sigma_{ij}^{0}+\sigma_{ij}\right)\alpha_{ij}^{\beta}-\tau_2^{p}\right]=\lambda_2\left\{\alpha_{ij}^{\beta}\left[\sigma_{ij}^{0}+C_{ijkl}(S_{klmn}-I_{klmn})\left(\sum_{\beta=1}^{3}\gamma^{\beta}\alpha_{mn}^{\beta}+\sum_{\beta=4}^{12}\gamma^{\beta}\alpha_{mn}^{\beta}-\bar{\varepsilon}_{mn}^{p}\right)\right]-\tau_2^{p}\right\},\ 4\le\beta\le 12. \tag{42}$$

We could only consider the equlibrium state, that is,

$$\begin{aligned}
&\lambda_1\left[\left(\sigma_{ij}^{0}+\sigma_{ij}\right)\alpha_{ij}^{\beta}-\tau_1^{p}\right]=0,\\
&\alpha_{ij}^{\beta}\left[\sigma_{ij}^{0}+C_{ijkl}(S_{klmn}-I_{klmn})\left(\sum_{\beta=1}^{3}\gamma^{\beta}\alpha_{mn}^{\beta}+\sum_{\beta=4}^{12}\gamma^{\beta}\alpha_{mn}^{\beta}-\bar{\varepsilon}_{mn}^{p}\right)\right]\\
&\quad-\tau_1^{p}=0,\quad 1\le\beta\le 3,\\
&\lambda_2\left[\left(\sigma_{ij}^{0}+\sigma_{ij}\right)\alpha_{ij}^{\beta}-\tau_2^{p}\right]=0,\\
&\alpha_{ij}^{\beta}\left[\sigma_{ij}^{0}+C_{ijkl}(S_{klmn}-I_{klmn})\left(\sum_{\beta=1}^{3}\gamma^{\beta}\alpha_{mn}^{\beta}+\sum_{\beta=4}^{12}\gamma^{\beta}\alpha_{mn}^{\beta}-\bar{\varepsilon}_{mn}^{p}\right)\right]\\
&\quad-\tau_2^{p}=0,\quad 4\le\beta\le 12.
\end{aligned} \tag{43}$$

In fact, eq. (43) is the same as the equations derived by the self-consistent approach established by many distinguished scholars, as summarized in Mura's book.

When the applied load reaches some critical value, the preferable slip system becomes active, and with the increase of the load, an increasingly orientation-preferable slip system becomes active. Thus, the true orientation distribution of the active slip system is evaluated with the increasing loading.

The self-consistent scheme is used to simulate the stress-strain behaviors for nano-twinned copper. In the equilibrium state, it can be assumed that each grain experiences a quasi-static process when the applied loading is increased. According to eq. (43), one had the increment equations for an isotropic elastic spherical grain

$$\Delta\sigma_{ij}^{0}\alpha_{ij}^{\beta}+2\alpha_{ij}^{\beta}G\left[1-\frac{2(4-5\nu)}{15(1-\nu)}\right]\left(\sum_{\beta=1}^{12}\Delta\gamma^{\beta}\alpha_{mn}^{\beta}-\Delta\bar{\varepsilon}_{mn}^{p}\right)=\Delta\tau_{\beta}^{p}, \tag{44}$$

where G is the shear modulus and ν is the Poisson's ratio. Eq. (44) could be solved iteratively at a given applied loading increment $\Delta\sigma_{ij}^{0}$ for all potentially active slip systems in each grain until a self-consistent solution of $\Delta\bar{\varepsilon}^{p}$ is obtained. The change of the macroscopic strain is calculated with

$$\Delta\bar{\varepsilon}_{ij}=C_{ijkl}^{-1}\Delta\sigma_{ij}^{0}+\Delta\bar{\varepsilon}_{ij}^{p}. \tag{45}$$

Thus, the macroscopic stress-strain response is obtained.

The controlling factors of the self-consistent calculation are the critical resolved shear stress for both the soft mode and the hard mode, which are the function of the plastic shear strain. In the implementation of the model, we adopted a hardening law that provided only self-hardening

$$\tau_{\beta}^{p}=\tau_{\beta}^{0}+\tau_{\beta}^{1}\left[1-\exp\left(-\frac{h_{\beta}\left|\gamma^{\beta}\right|}{\tau_{\beta}^{1}}\right)\right]. \tag{46}$$

Therefore, the linear approximation of $\Delta\tau_{\beta}^{p}$ with respect to the plastic shear strain can be expressed as:

$$\Delta\tau_{\beta}^{p}=h_{\beta}\exp\left(-\frac{h_{\beta}\left|\gamma^{\beta}\right|}{\tau_{\beta}^{1}}\right)\cdot\Delta\left|\gamma^{\beta}\right|. \tag{47}$$

In the calculations, the orientation distribution was represented by 4800 copper grains, for which the twin plane orientation of each grain was described by three random Euler angles. The diameter of each grain was assumed to be 400 nm so that the initial critical resolved shear stress of the soft mode τ_{soft}^{0} was taken to be 67 MPa [18]. τ_{hard}^{0} could be determined with the Hall-Petch relationship:

$$\tau_{\mathrm{hard}}^{0}=\tau_0+k/\sqrt{d_{\mathrm{twin}}}, \tag{48}$$

where d_{twin} represents the twin spacing. Figure 5 shows the tensile strain-stress curves estimated by the self-consistent model, along with the experimental results [18]. The main trends of the strain-stress responses in terms of the twin spacing were captured. The material constants for the self-consistent calculation are as follows: Y=110 GPa, G=46 GPa, ν=0.34, τ_0=15 MPa [19], k=1.6 GPa·nm$^{1/2}$[20], h_{β}=

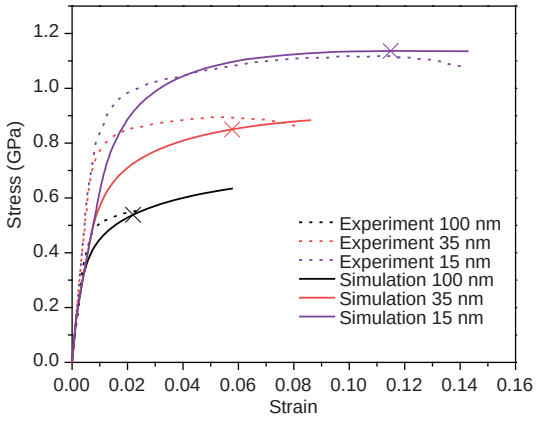

Figure 5 (Color online) Comparison of the simulated and experimental tensile stress-strain curves of nano-twinned copper with different twin spacings (100 nm, 35 nm, 15 nm). The experimental data is available in ref. [18]. The symbol X denotes the point whose strain was equal to the experimentally observed strain at the tensile strength. The corresponding stresses for the three X were 540 MPa (experiment: 552 MPa) for d_{twin}=100 nm, 852 MPa (experiment: 897 MPa) for d_{twin}=35 nm and 1136 MPa (experiment: 1118 MPa) for d_{twin}=15 nm.

1 GPa, and τ_β^1=0.2.

If one is only interested in the ultimate strength, one can take the second variation of the right-hand terms of eq. (42) and make it equal to zero. One can then find the inflection point in the Gibbs free energy curve that corresponds to the ultimate strength point. One can find that for this case, the ultimate strength can be reached when the slip strain approaches infinity.

3.5 Comparison of local strength criterion and global strength criterion

Most empirical strength criteria are local criteria. whereas, many criteria in fracture mechanics such as the energy release rate criterion and J-integral belong to the global strength criterion. To show how different the prediction by the local criterion and the global criterion, in this work two cases will be considered: one is a hole with different sizes in an infinite plate under the uniaxial tensile loading; the other is our recent experimental results on the strength of lithium niobite crystal specimens with different sizes of notches[1)]. The maximum stress strength criterion is used as the local criterion, and compared with the present global strength criterion.

3.5.1 A circular hole with different sizes in an infinite plate under the uniaxial loading

(1) Local criterion based on the maximum stress

For an infinite plate with a circular hole under the uniaxial loading (Figure 6(a)), the maximum stress will arise at the boundary of the hole, and the maximum stress can be given by the theory of elasticity as follows:

$$\sigma_{\max}=3\sigma_s=\sigma_c;\ \sigma_s=\frac{1}{3}\sigma_c, \tag{49}$$

which means that the strength does not depend on the size of the hole.

(2) Global criterion based on the energy approach

According to the VPEC, one can assume that the specimen breaks from the tiny crack at the boundary (Figure 6(b)), then one can establish the energy criterion, which is the same as the energy release rate criterion of fracture mechanics as follow:

$$\begin{aligned} &K_I=F\sigma_s\sqrt{\pi(a+\Delta a)}=K_{IC},\\ &\sigma_s=\frac{K_{IC}}{F\sqrt{\pi(a+\Delta a)}}=\frac{K_{IC}}{F\sqrt{\pi a}}\propto(a)^{-1/2}. \end{aligned} \tag{50}$$

It is very clear the strength should be proportional to $(a)^{-1/2}$. The author has not found the experimental data in the references to check the predictions, but it is not difficult to obtain the experimental results.

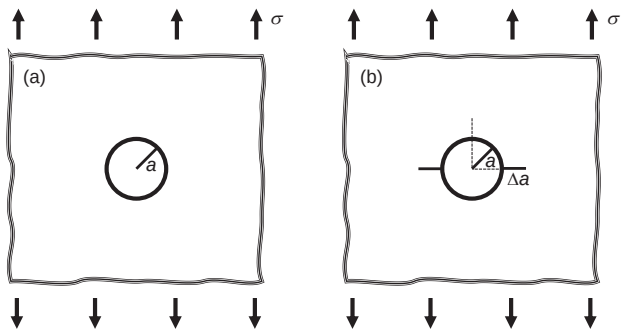

Figure 6 Schematic of a circular hole in an infinite plate (a) without and (b) with the tiny crack under uniaxial loading.

3.5.2 The strength of single crystal lithium niobate ($LiNbO_3$) specimen with different notches

Recently, the strength properties of *c*-axis oriented $LiNbO_3$ has been experimentally investigated by our group[1)]. Three-point bend testing was carried out with single-edge-notched bend (SENB) specimens at room temperature. Polarized and non-polarized SENB specimens with different depth of U-shaped notch were prepared and tested. In this work the experimental data will be used to verify the local and global strength model.

(1) Specimens preparation

The single crystal $LiNbO_3$ for the experiment was produced by using the Czochralski method in our laboratory. Crystal orientation was determined by using the X-ray crystal orientation tool. Bulk $LiNbO_3$ polarization process was carried out in muffle furnace. Temperature was increased from room temperature to 1200°C in 20 h. Then, a 5.0 mA/cm^2 direct current was applied in the *c*-axis direction for 8 h. Finally, temperature was cooled down from 1200°C to room temperature in 30 h. According to the classic three-point bending specimen design requirements, the shape of specimen was designed as Figure 7: $1\leq W/B\leq 4$, $S=4W$, where W is width, and B is thickness. The sizes of W and B were machined to about 4.0 and 1.7 mm, so the nominal span was set as 16.0 mm. The depth of notch, a, was machined to about 0.8, 1.3, 1.7, 2.0 mm by the wire cutting with a thickness of 0.3 mm diamond line (Figure 8(a)). In order to use the DICM to measure deformation, the test piece needs to make a CSI professional speckle (Figure 8(b)). The length of test specimens is shown as Figure 8(c).

(2) Experimental results

The obtained experimental results are shown in Tables 1 and 2.

(3) Local strength criterion based on the maximum stress

For the experimental setup shown in Figure 7, the maximum stress should arise the root of the notch, and the approximate relationship between the applied loading P and the

1) G. Lian, B. Wang, and Y. Liu, Eng. Fract. Mech., 2020 (to be published).

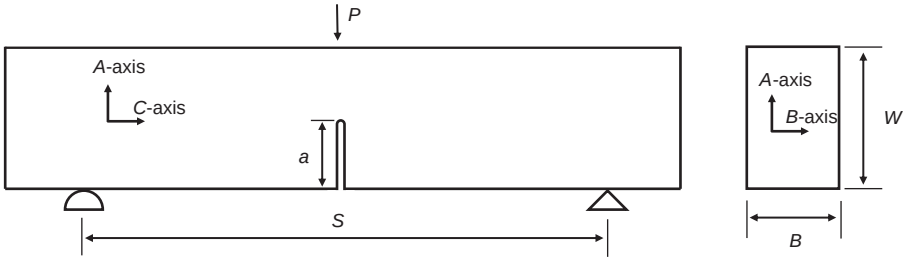

Figure 7 Experimental setup and geometry of SENB specimen.

maximum stress has been derived [21], which can be written in the form as:

$$\sigma_{\max}=\sigma_c=\frac{3P_cS}{2BW^2}\frac{a+\rho}{\sqrt{\rho^2+2a\rho}}\left(\frac{W-a}{W-a-\rho}\right)^2 \times\left[2\left(1-\frac{2\rho}{W}\right)^{-1}+\left(1-\frac{2\rho}{W}\right)^2\right]f(a/W),$$
$$f\left(\frac{a}{W}\right)=1.12-1.40\left(\frac{a}{W}\right)+7.33\left(\frac{a}{W}\right)^2 -13.08\left(\frac{a}{W}\right)^3+14\left(\frac{a}{W}\right)^4. \quad (51)$$

The critical stress is obtained as the average value of the maximum stress at the failure point, which is $\sigma_c = 294$ MPa. Then the predicted applied maximum loading versus a is shown in Figure 9.

(4) Global strength criterion based on the energy approach

As explained above, the global energy criterion is the same as the energy release rate or the stress intensity factor criterion for a specimen with a crack. To simplify the derivation, it is assumed that a pre-existing tiny crack is located at the tip of the notch. Then from the fracture mechanics, the stress intensity factor can be written in the form as:

$$\begin{cases} K_I=\dfrac{3P_cS}{2BW^2}\sqrt{\pi(a+a_0)}\cdot f\left(\dfrac{a'}{W}\right)=K_{IC}, \\ f\left(\dfrac{a'}{W}\right)=1.12-1.40\left(\dfrac{a+a_0}{W}\right)+7.33\left(\dfrac{a+a_0}{W}\right)^2 \\ \qquad -13.08\left(\dfrac{a+a_0}{W}\right)^3+14\left(\dfrac{a+a_0}{W}\right)^4. \end{cases} \quad (52)$$

It was found that $K_{IC} = 108.25$ MPa mm$^{\frac{1}{2}}$, a_0=0.126 mm, the maximum relative error is less than 2%. The maximum applied loading versus a can be obtained, and shown in Figure 9, together with the experimental data.

It is very clear that the global energy criterion gives the more reasonable results. One can imagine that if the critical maximum stress is determined by the strength value of the specimen without the notch, the local strength theory gives much more unreasonable results.

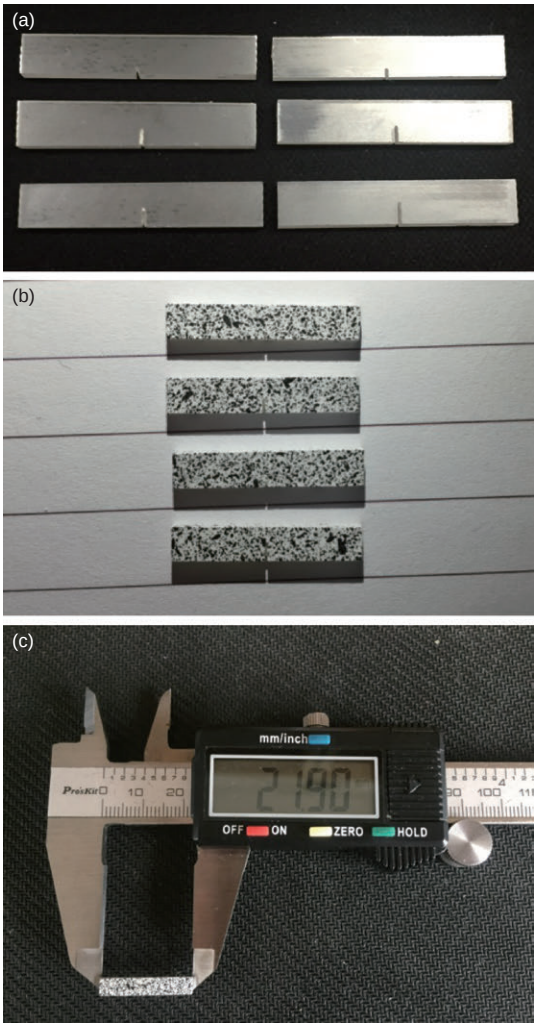

Figure 8 (Color online) (a) Specimens with different depth of U-shaped notch, (b) specimens with speckle, (c) the size of specimens.

4 Some concluding remarks

In this research, the main goal was to reconsider the strength problem in mechanics. Based on the virtual failure mechanism, the evolution equation was established based on rational nonequilibrium thermodynamics. Then, the strength properties could be determined using the stability analysis. In fact, if one is only interested in the strength value, one can use the second-order variation of the free energy to find out

Table 1 Specific data of the non-polarized specimens

Specimen number	S (mm)	W (mm)	B (mm)	a (mm)	P_{max} (N)	a/W
1-1	16	3.90	1.76	0.8	66.52	0.21
1-2	16	4.00	1.71	1.0	60.38	0.25
1-3	16	4.03	1.73	1.3	50.83	0.32
1-4	16	4.20	1.76	1.6	47.20	0.38
1-5	16	4.13	1.70	2.0	32.85	0.48

Table 2 Specific data of the polarized specimens

Specimen number	S (mm)	W (mm)	B (mm)	a (mm)	P_{max} (N)	a/W
2-1	16	4.20	1.73	0.8	77.52	0.19
2-2	16	4.03	1.66	0.8	66.82	0.20
2-3	16	4.10	1.70	1.5	46.49	0.37
2-4	16	4.30	1.73	1.7	47.11	0.40

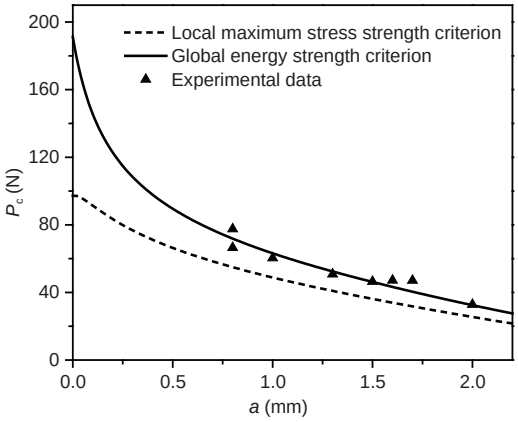

Figure 9 Comparison of the local maximum stress criterion and global energy criterion with the experimental data of lithium niobite single crystals.

the unstable equilibrium point as shown in nonequilibrium thermodynamics without need to consider the evolution equations [4]. From such an energetic idea, it was very clear that the strength property was a global behavior, and at the critical state, all of the points in the specimen were all closely correlated. It was not my purpose to show that all the conventional local strength theories are incorrect. In fact, for example, the stress intensity factor criterion in fracture mechanics proposed by Irwin [22] was a very clever idea. It is a local criterion. However, it is also directly related to the global criterion, the energy release rate criterion. I only wanted to demonstrate that the strength was intrinsically a global property, and that the fundamentals of the local strength criteria based on the maximum stress, stress combination, and other factors might need revision. From comparison with our experimental data of the lithium niobite specimens with notches of different sizes, the pre-existing tiny crack at the root of the notches seems the key factor, in fact, it is not the main purpose here. Whereas it is very clear that many fracture criteria, such as the energy release rate criterion and J-integral criterion should give the same results as the energy theory developed here, therefore we adopted the fracture mechanics analysis to deal with the strength problem for simplification, and the results are satisfactory, which means that the pre-existing defect assumption should be reasonable, since at least the real materials are not real continuum. To satisfy the engineering demands, it is needed to develop some methodologies based on rational thermodynamics. In fact, based on the energy methodology, one can do many reasonable predictions for different problems [23-31].

Finally, one should notice that the examples considered in this work are familiar to the scholars in this area, and they are only the explanations for the main ideas of the author. It is the main purpose to find out the intrinsic characteristics of material failure, establish its thermodynamic foundation, and to help researchers to formulate their strength theories on a rational base, instead of depending on some empirical parameters or criteria.

This work was supported by the National Natural Science Foundation of China (Grant Nos. 11832019, 11472313, and 13572355). Dr. JiaPeng Chen, my former PhD student, and now my post-doctoral associate helped me to carry out the detail calculation shown in Figure 5, and help me to draw the Figures 6 and 9, and Mr. Jun Hui, my PhD student, helped me to collect the data and draw the Figures 1-4. The author appreciated their help very much.

1 A. A. Griffith, Phil. Trans. R. Soc. Lond. A **221**, 163 (1921).
2 K. Lu, L. Lu, and S. Suresh, Science **324**, 349 (2009).
3 R. H. Telling, C. J. Pickard, M. C. Payne, and J. E. Field, Phys. Rev. Lett. **84**, 5160 (2000).
4 D. Kondepudi, and I. Prigogine, *Modern Thermodynamics: From Heat Engines to Dissipative Structures* (John Wiley & Sons, Chichester, 2014).
5 Z. P. Bažant, Archive Appl. Mech. (Ingenieur Archiv) **69**, 703 (1999).
6 A. Taloni, M. Vodret, G. Costantini, and S. Zapperi, Nat. Rev. Mater. **3**, 211 (2018).

7 B. Sun, *Dimensinal Analysis and Lie Group* (in Chinese) (China High Education Press, Beijing, 2016).
8 Z. P. Bažant, I. M. Daniel, and Z. Li, J. Eng. Mater. Tech. **118**, 317 (1996).
9 C. C. Vu, J. Weiss, O. Plé, D. Amitrano, and D. Vandembroucq, J. Mech. Phys. Solids **121**, 47 (2018).
10 P. B. Zdeněk, and M. T. Kazemi, J. Am. Cream. Soc. **73**, 1841 (1990).
11 S. Bandis, A. C. Lumsden, and N. R. Barton, Int. J. Rock Mech. Min. Sci. GeoMech. Abstracts **18**, 1 (1981).
12 B. Wang, and J. P. Boehler, J. Mech. Phys. Solids **44**, 2103 (1996).
13 T. Mura, *Micromechanics of Defects in Solids* (Kluwer Academic Publisher, Dordrecht, Boston, London, 1987).
14 C. Unger, and W. Klein, Phys. Rev. B **29**, 2698 (1984).
15 L. Lu, X. Chen, X. Huang, and K. Lu, Science **323**, 607 (2009).
16 Z. Cheng, H. Zhou, Q. Lu, H. Gao, and L. Lu, Science **362**, 6414 (2018).
17 X. Li, Y. Wei, L. Lu, K. Lu, and H. Gao, Nature **464**, 877 (2010).
18 M. Dao, L. Lu, Y. F. Shen, and S. Suresh, Acta Mater. **54**, 5421 (2006).
19 B. Clausen, T. Lorentzen, and T. Leffers, Acta Mater. **46**, 3087 (1998).
20 R. A. Masumura, P. M. Hazzledine, and C. S. Pande, Acta Mater. **46**, 4527 (1998).
21 M. Liu, Y. Gan, D. A. H. Hanaor, B. Liu, and C. Chen, Eng. Fract. Mech. **149**, 134 (2015).
22 G. R. Irwin, ASME J. Appl. Mech. **24**, 109 (1957).
23 J. Chen, B. Wang, and Y. Hu, J. Mech. Phys. Solids **107**, 451 (2017), arXiv: 1610.01467.
24 J. P. Chen, and B. Wang, Sci. China-Phys. Mech. Astron. **62**, 954611 (2019).
25 W. Yang, H. T. Wang, T. F. Li, and S. X. Qu, Sci. China-Phys. Mech. Astron. **62**, 014601 (2019).
26 R. F. Zhang, C. L. Ren, J. W. Feng, and Y. Q. Ma, Sci. China-Phys. Mech. Astron. **62**, 117012 (2019), arXiv: 1903.06387.
27 K. M. Liew, Z. Pan, and L. W. Zhang, Sci. China-Phys. Mech. Astron. **63**, 234601 (2020).
28 Y. Sun, K. Y. Zeng, and T. Li, Sci. China-Phys. Mech. Astron. **63**, 278701 (2020).
29 Z. Wu, S. Huang, J. Ding, W. Wang, and X. Luo, Sci. China-Phys. Mech. Astron. **61**, 114712 (2018).
30 F. Berto, and P. Lazzarin, Mat. Sci. Eng. R **75**, 1 (2014).
31 C. C. Yang, and Y.-W. Mai, Mat. Sci. Eng. R **79**, 1 (2014).

Appendix Eshelby's tensor for spherical inclusion and identity tensor

For spherical grain, Eshelby's tensor only depends on Poisson's ratio as follows:

$$S_{1111}=S_{2222}=S_{3333}=\frac{7-5\nu}{15(1-\nu)},$$
$$S_{1122}=S_{2222}=S_{3311}=S_{1133}=S_{2211}=S_{3322}=\frac{5\nu-1}{15(1-\nu)}, \quad \text{(a1)}$$
$$S_{1212}=S_{2323}=S_{3131}=\frac{7-5\nu}{15(1-\nu)},$$

where ν is Poisson's ratio, and the identity tensor is

$$I_{ijkl}=\frac{1}{2}(\delta_{ik}\delta_{jl}+\delta_{il}\delta_{jk}), \quad \text{(a2)}$$

where δ_{ij} is Kronecker delta.